

See discussions, stats, and author profiles for this publication at: <https://www.researchgate.net/publication/265055552>

# Lithiation-Induced Shuffling of Atomic Stacks

ARTICLE *in* NANO LETTERS · AUGUST 2014

Impact Factor: 13.59 · DOI: 10.1021/nl502347z · Source: PubMed

---

CITATIONS

2

READS

82

## 11 AUTHORS, INCLUDING:



[Yihan Zhu](#)

King Abdullah University of Science and Techn...

45 PUBLICATIONS 977 CITATIONS

[SEE PROFILE](#)



[Hasti Asayesh-Ardakani](#)

Michigan Technological University

9 PUBLICATIONS 47 CITATIONS

[SEE PROFILE](#)



[Yu Han](#)

King Abdullah University of Science and Techn...

144 PUBLICATIONS 6,068 CITATIONS

[SEE PROFILE](#)



[R. F. Klie](#)

University of Illinois at Chicago

212 PUBLICATIONS 2,667 CITATIONS

[SEE PROFILE](#)

## Lithiation-Induced Shuffling of Atomic Stacks

Anmin Nie,<sup>†,‡,§</sup> Yingchun Cheng,<sup>‡,§</sup> Yihan Zhu,<sup>||,§</sup> Hasti Asayesh-Ardakani,<sup>†</sup> Runzhe Tao,<sup>#</sup> Farzad Mashayek,<sup>¶</sup> Yu Han,<sup>||</sup> Udo Schwingenschlögl,<sup>‡</sup> Robert F. Klie,<sup>#</sup> Sreeram Vaddiraju,<sup>⊥</sup> and Reza Shahbazian-Yassar<sup>\*,†,‡,¶,||</sup>

<sup>†</sup>Department of Mechanical Engineering-Engineering Mechanics, Michigan Technological University, 1400 Townsend Drive, Houghton, Michigan 49931, United States

<sup>‡</sup>Department of Physical Science and Engineering, King Abdullah University of Science & Technology, Thuwal, 23955-6900, Kingdom of Saudi Arabia

<sup>||</sup>Advanced Membranes and Porous Materials Center, Physical Sciences and Engineering Division, King Abdullah University of Science & Technology, Thuwal, 23955-6900, Kingdom of Saudi Arabia

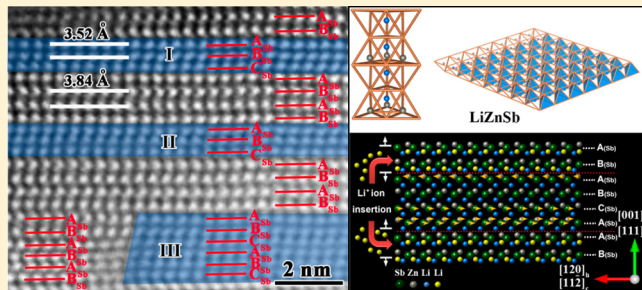
<sup>⊥</sup>Artie McFerrin Department of Chemical Engineering, Texas A&M University, 3122 TAMU, College Station, Texas 77843, United States

<sup>#</sup>Department of Physics, University of Illinois at Chicago, Chicago, Illinois 60607, United States

<sup>¶</sup>Mechanical and Industrial Engineering Department, University of Illinois at Chicago, Chicago, Illinois 60607, United States

### S Supporting Information

**ABSTRACT:** In rechargeable lithium-ion batteries, understanding the atomic-scale mechanism of Li-induced structural evolution occurring at the host electrode materials provides essential knowledge for design of new high performance electrodes. Here, we report a new crystalline–crystalline phase transition mechanism in single-crystal Zn–Sb intermetallic nanowires upon lithiation. Using *in situ* transmission electron microscopy, we observed that stacks of atomic planes in an intermediate hexagonal (*h*-)LiZnSb phase are “shuffled” to accommodate the geometrical confinement stress arising from lamellar nanodomains intercalated by lithium ions. Such atomic rearrangement arises from the anisotropic lithium diffusion and is accompanied by appearance of partial dislocations. This transient structure mediates further phase transition from *h*-LiZnSb to cubic (*c*-)Li<sub>2</sub>ZnSb, which is associated with a nearly “zero-strain” coherent interface viewed along the [001]<sub>*h*</sub>/[111]<sub>*c*</sub> directions. This study provides new mechanistic insights into complex electrochemically driven crystalline–crystalline phase transitions in lithium-ion battery electrodes and represents a noble example of atomic-level structural and interfacial rearrangements.



**KEYWORDS:** lithium-ion batteries, *in situ* STEM, atomic scale, phase transition, Zn<sub>4</sub>Sb<sub>3</sub> nanowires

Numerous research efforts have been devoted toward the next generation of lithium ion batteries (LIBs) due to the ever-growing need for high specific energy density and good cycling performance.<sup>1–3</sup> The main challenge facing LIBs is the discovery of new electrode materials with promising electrochemical lithium ion storage properties and a mechanistic understanding of the reactions taking place in the cells.<sup>4,5</sup> For next generation LIBs, electrochemically driven phase transitions are widely involved in the electrode materials and also closely linked with LIBs performance.<sup>6–8</sup> Recent *in situ* transmission electron microscopy (TEM) works have documented Li-induced crystalline to amorphous phase transitions<sup>9,10</sup> or Li-induced atomic ordering within amorphous matrix.<sup>11,12</sup> However, direct atomic-scale observations of electrochemically driven crystalline–crystalline phase transition in LIBs have hardly been achieved.<sup>13</sup>

Intermetallic alloys often undergo electrochemically driven crystalline–crystalline phase transitions that results in complex charge–discharge cycling performance. In particular, Sb-based intermetallic alloys have received imminent attention in rechargeable battery community for their high theoretical capacities and suitable operating voltages.<sup>14–16</sup> New and elegant concepts are introduced behind the design of these Sb-based intermetallic electrodes due to the strong structural relationship with their lithiated products. For instance, SnSb electrodes provide a high capacity and controllable volume expansion due to both Sn and Sb metals reacting with Li and distributing a ductile Sn phase during cycling.<sup>17,18</sup> A reversible process of lithium insertion and metal extrusion was suggested

**Received:** June 22, 2014

**Revised:** August 14, 2014



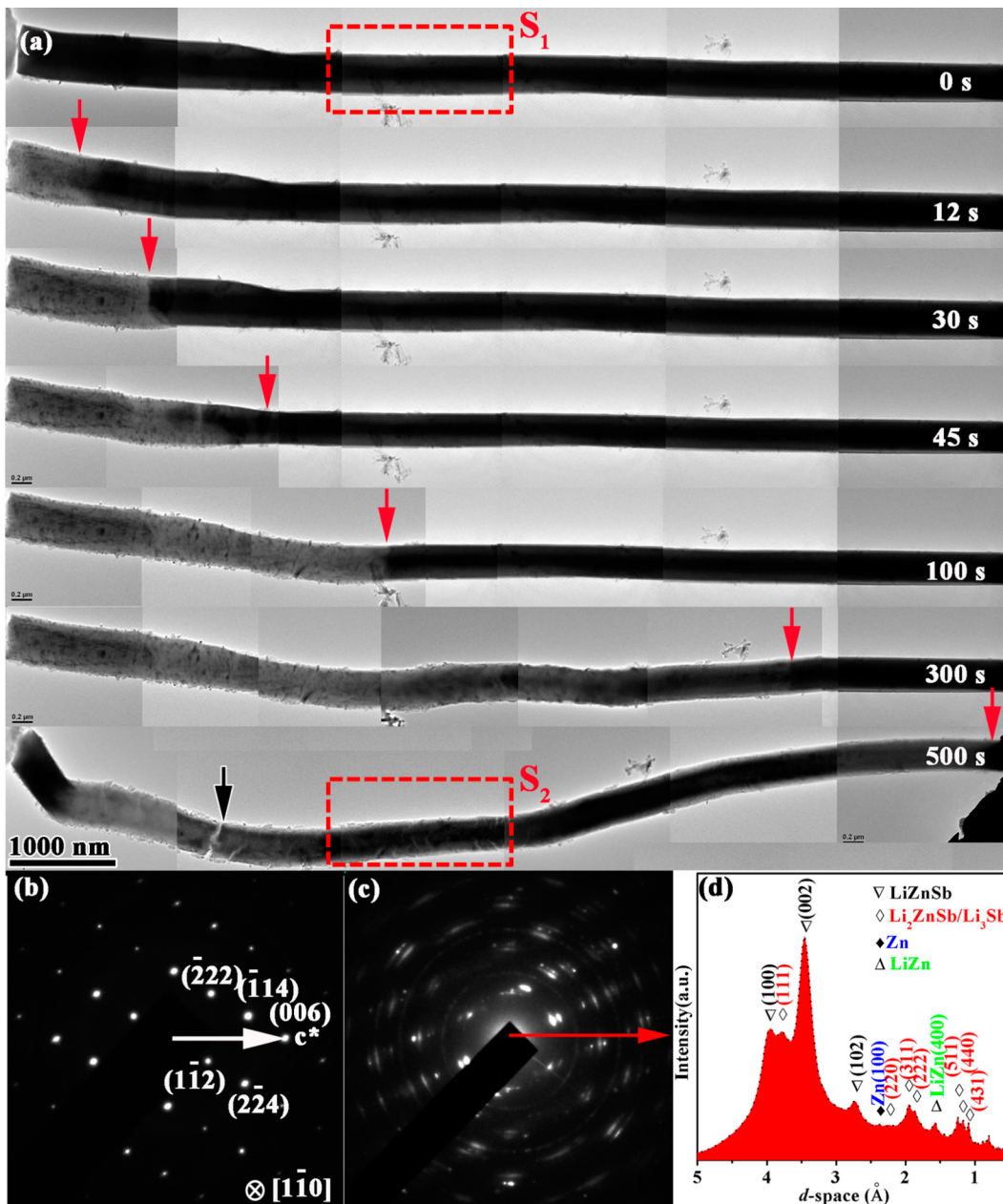


**Figure 1.** Morphology and microstructural evolution of individual  $\text{Zn}_4\text{Sb}_3$  nanowires during charging against lithium metal. (a) Time-lapse morphology evolution of the  $\text{Zn}_4\text{Sb}_3$  nanowire. As the reaction front (marked by red arrow) passed by, the nanowire expanded both in radial and axial direction. Cracks and some nanoparticles formed at the late stage of lithiation. (b) SAED pattern taken from area  $S_1$  (marked in (a)) with  $[1\bar{1}0]$  zone axis before reaction front passing by. (c) SAED pattern taken from area  $S_2$  (marked in (a)) after the lithiation. (d) Intensity profile from the electron diffraction pattern shown in (c) along the red arrow line. The peaks corresponding with the specific rings in the electron diffraction pattern are indexed to be  $\text{LiZnSb}$ ,  $\text{Zn}$ ,  $\text{LiZn}$ , and either  $\text{Li}_2\text{ZnSb}$  or  $\text{Li}_3\text{Sb}$ .

in  $\text{Cu}_2\text{Sb}$  electrodes with a stable face-centered-cubic (*fcc*) Sb host framework for both the incoming and extruded metal atoms.<sup>19</sup> In addition, quasi-intercalation concept was proposed in orthorhombic  $\text{ZnSb}$  due to the layered structures of  $\text{ZnSb}$  and hexagonal  $\text{LiZnSb}$  (*h*- $\text{LiZnSb}$ ).<sup>14</sup> Most of these mechanisms were proposed in light of ex situ X-ray diffraction (XRD), which has intrinsic limitations in resolving aperiodic components like strains, defects, and disorders at high spatial resolution. Therefore, the dynamic nature of these interesting phenomena does need to be further explored by *in situ* tools.

In this work, we reveal a new type of lithiation-triggered crystalline–crystalline phase transitions at atomic-scale for  $\text{Zn}$ –

Sb alloys. Taking advantage of an aberration-corrected scanning transmission electron microscope (STEM) with potential to identify atomic distances as small as 0.7 Å<sup>20</sup> and image the light elements such as oxygen,<sup>21</sup> lithium,<sup>22,23</sup> and hydrogen<sup>24</sup> in crystal structures by embracing the annular bright field (ABF) STEM technique, we directly observed the dynamics of lithiation in individual single-crystal  $\text{Zn}_4\text{Sb}_3$  nanowires. The kinetics of lithiation was found to be highly anisotropic and relevant to the interfacial structures of the reaction front at different stages of lithiation. Atom-resolved images of interfacial structures captured at different lithiation stages clearly reveal that the initial lithiation of  $\text{Zn}_4\text{Sb}_3$  nanowire proceeded via

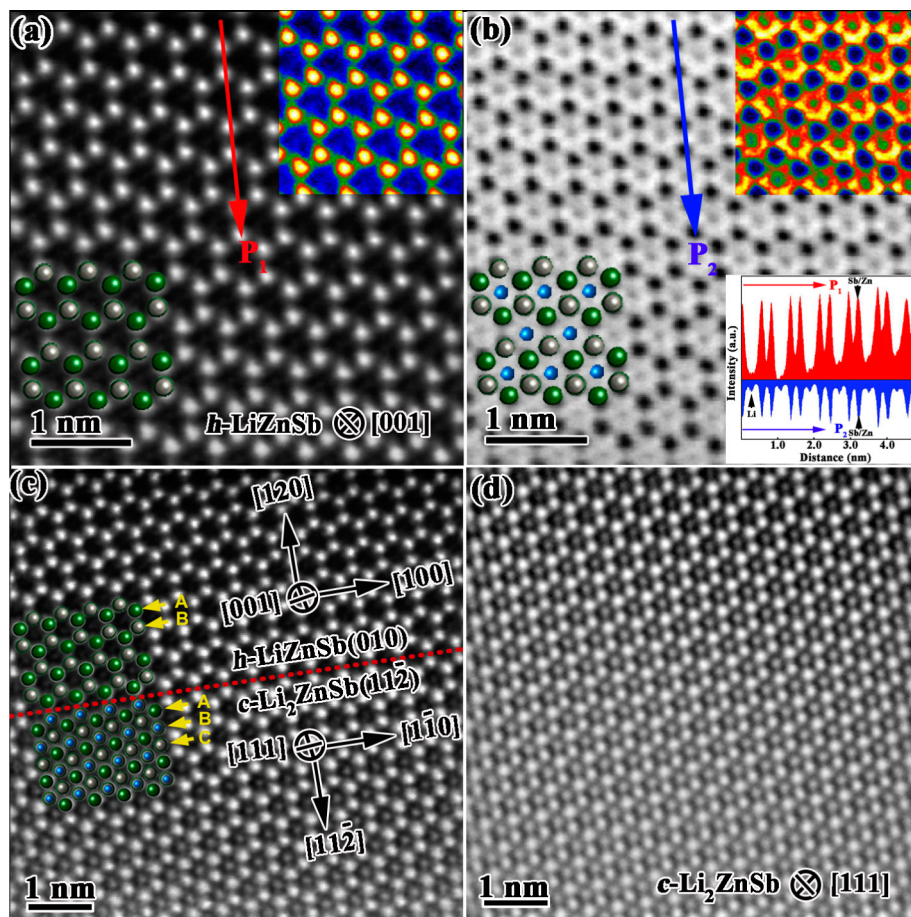


**Figure 2.** Atomic resolution STEM images of phase transition from *h*-LiZnSb to *c*-Li<sub>2</sub>ZnSb. (a) Atomic resolution HAADF image for *h*-LiZnSb along [001]<sub>h</sub> zone axis. Inset is the corresponding colored HAADF image. (b) ABF image for *h*-LiZnSb along [001]<sub>h</sub> zone axis. Top inset is the corresponding colored ABF image. The colored ABF image highlights the Li visibility as green. Bottom inset corresponds to intensity profiles along P<sub>1</sub> and P<sub>2</sub> from HAADF and ABF images, respectively. The presence of Li atoms is clearly detectable in the intensity profile along P<sub>2</sub>. (c) Atomic resolution HAADF image of the interfacial structure between *h*-LiZnSb (Above red dotted line and along [001]<sub>h</sub> zone axis) and *c*-Li<sub>2</sub>ZnSb (Below red dotted line and along [111]<sub>c</sub> zone axis). The two areas show different stacking sequences (Top: ABABAB, Bottom: ABCABC). (d) Atomic resolution HAADF image shows *c*-Li<sub>2</sub>ZnSb [111]<sub>c</sub> projection after the interface migration.

formation of intermediate *h*-LiZnSb and cubic Li<sub>2</sub>ZnSb (*c*-Li<sub>2</sub>ZnSb) phases before transforming to Li<sub>3</sub>Sb with Zn extrusion. Interestingly, we found that the phase transition from *h*-LiZnSb to *c*-Li<sub>2</sub>ZnSb is triggered by stress-induced shuffling of stacked atomic layers due to the anisotropic transport of lithium ions.

The general chemical and microstructural features of pristine Zn<sub>4</sub>Sb<sub>3</sub> nanowire are presented in Figure S1 and S2 (Supporting Information). The Zn<sub>4</sub>Sb<sub>3</sub> nanowires are confirmed to be monocrystalline with the [001] growth direction. The Zn<sub>4</sub>Sb<sub>3</sub> nanowire was subjected to lithiation process by using an *in situ* electrochemical cell<sup>9</sup> inside TEM (Supporting Information Figure S3). Figure 1a (Supporting Information Movie S1) shows the propagation of the reaction front in a Zn<sub>4</sub>Sb<sub>3</sub> nanowire during lithiation. As the reaction front (marked by the red arrow) propagated along the longitudinal direction, the TEM image contrast changed from dark to gray due to phase transition. After lithiation, this nanowire elongated by about 10%, the diameter increased by about 15%, and the total volume expanded by about 45%. In addition, nanocracks were formed in the lithiated section of the nanowire matrix as pointed out by the black arrow in Figure 1a. More detailed structure and phase characterization before and after lithiation

is given by selected area electron diffraction (SAED) patterns (Figure 1b and c). Figure 1b shows the SAED pattern taken along the [110] zone axis from the section of the nanowire marked as S<sub>1</sub>. From the SAED pattern, it can be conclude that the nanowire was monocrystalline with a [001] growth direction before lithiation, which is consistent with the atomic-resolution STEM images (Supporting Information Figure S2). After lithiation, the SAED pattern (Figure 1c) taken from the same area of the nanowire marked as S<sub>2</sub> shows diffraction rings, which indicates the formation of nanocrystals of new phases. The corresponding intensity profile (Figure 1d) along the red arrow line in Figure 1c shows peaks at different position (*d*-spacing), evidencing the formation of Zn, *h*-LiZnSb, *c*-Li<sub>2</sub>ZnSb, Li<sub>3</sub>Sb, and LiZn. Due to close *d*-spacing, it is challenging to explicitly distinguish between *c*-Li<sub>2</sub>ZnSb (S.G. F43m, *a* = 6.47 Å, JCPDS Card No.71-0222) and Li<sub>3</sub>Sb (S.G. Fm3m, *a* = 6.57 Å, JCPDS Card No. 04-0791) phases from the intensity profile of the SAED pattern (Supporting Information Figure S4), which is straightforward, however, for high-resolution imaging.

Followed by the electrochemically driven solid-state amorphization of Zn<sub>4</sub>Sb<sub>3</sub>, nucleation and growth of *h*-LiZnSb nanocrystals were observed in the lithiated amorphous

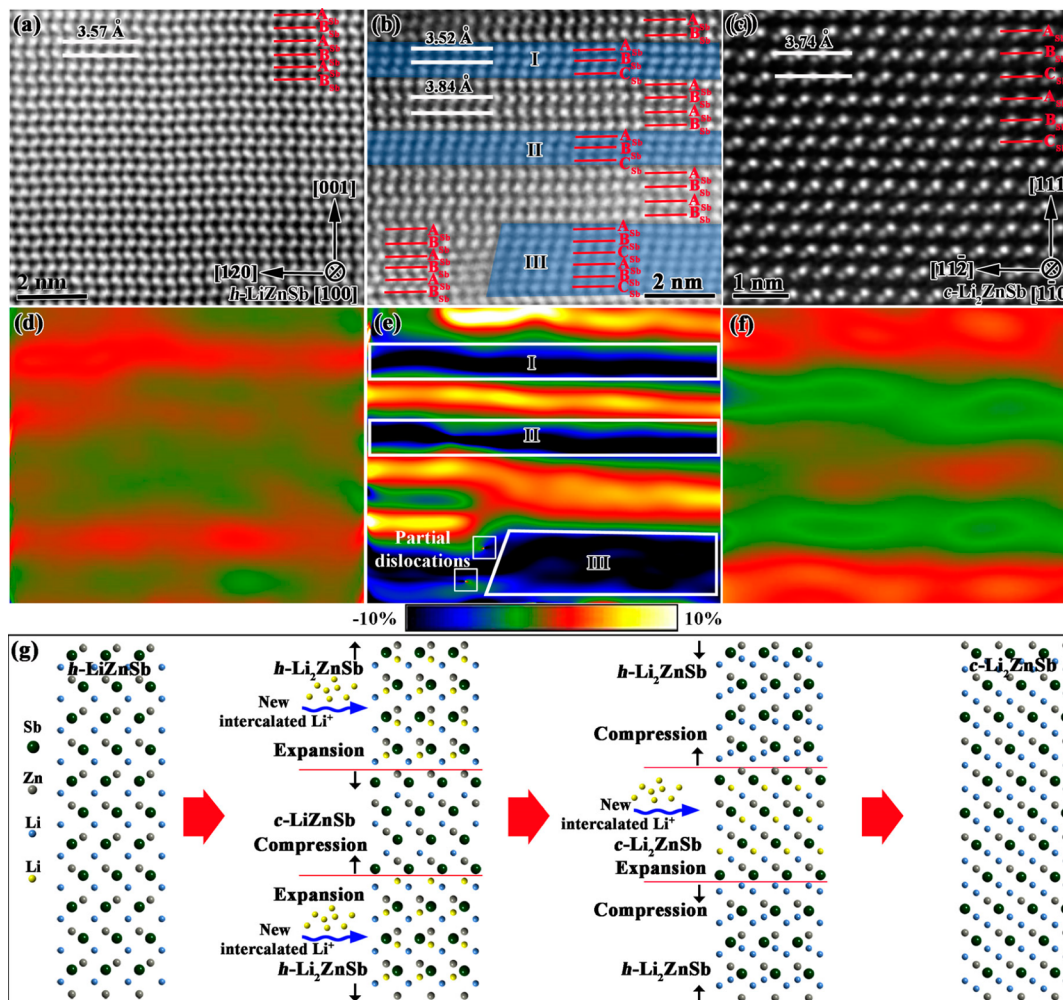


**Figure 3.** Direct imaging of phase transition from *h*-LiZnSb to *c*-Li<sub>2</sub>ZnSb. (a) Atomic resolution HAADF image showing *h*-LiZnSb structure viewed from [100]<sub>h</sub> direction. The Sb atom layers show ABABAB stacking sequence along [001]<sub>h</sub> direction. (b) Atomic resolution HAADF image showing intermediate structure from *h*-LiZnSb to *c*-Li<sub>2</sub>ZnSb. The domains with the ABC stacking sequence, which are highlighted by blue color. (c) Atomic resolution HAADF image of perfect *c*-Li<sub>2</sub>ZnSb structure along [111]<sub>c</sub> direction. The Sb layers show ABCABC stacking sequence along [111]<sub>c</sub> direction. (d) Strain mapping along [001]<sub>h</sub> direction of the *h*-LiZnSb structure calculated by using GPA from HAADF image (a). (e) Strain mapping normal to the stacking Sb layers of the intermediate structure calculated by using GPA from HAADF image (b). (f) Strain mapping along [111]<sub>c</sub> direction of the *c*-Li<sub>2</sub>ZnSb structure calculated by using GPA from HAADF image (c). The color scale is from -10% to 10%. (g) Schematic representation of phase transition from *h*-LiZnSb to *c*-Li<sub>2</sub>ZnSb. Yellow atoms indicate the new coming lithium ion and black arrows show the stress direction. Here, the formulas of LiZnSb and Li<sub>2</sub>ZnSb indicate nonintercalated and intercalated domains, respectively.

$\text{Li}_x\text{Zn}_4\text{Sb}_3$  matrix (Supporting Information Figure S5 and S6). Figure 2 shows atomic resolution high angle annular dark field (HAADF) and corresponding ABF images of a crystalline particle inside the lithiated nanowire, which later was identified as *h*-LiZnSb (S.G. P6<sub>3</sub>mc, JCPDS Card No. 34-0508) structure viewed along the [001]<sub>h</sub> direction. Due to the Z<sup>1,7</sup> dependence of HAADF contrast,<sup>25</sup> the light elemental atoms (such as Li and O) can hardly gain intensity in the HAADF image. Thus, in the HAADF image (Figure 2a), bright spots correspond to the overlapped Sb (Zn) atomic columns with the corresponding intensity line profile along direction P<sub>1</sub> as shown in the inset of Figure 2b. A false-colored HAADF image with more comprehensible contrast was inserted into Figure 2a. The Sb and Zn atomic-columns cannot be discriminated due to the overlap of them along the [001] zone axis. This well arrangement is also revealed by the intensity line profile along direction P<sub>2</sub> in the inset of the ABF image in Figure 2b. In comparison with profile P<sub>1</sub> in HAADF image, the Li atom columns can be directly observed in profile P<sub>2</sub>. Actually, the *h*-

LiZnSb structure can be derived by filling one-half of the tetrahedral voids periodically with the Zn-cations and all the octahedral voids with Li ions in an hexagonal close-packed (*hcp*-type) Sb sublattice (Supporting Information Figure S7). The *h*-LiZnSb phase is made of Zn/Sb/Li atomic layers stacked periodically along the [001]<sub>h</sub> direction, where Zn/Sb atoms alternatively occupy the A/B sites while Li atoms occupy the C sites. Here, A, B, and C refer to distinct atomic layers perpendicular to the stacking direction.

After further lithiation, the phase transition from *h*-LiZnSb to *c*-Li<sub>2</sub>ZnSb was observed. The *c*-Li<sub>2</sub>ZnSb phase consists of a more densely packed lattice where Zn and Li atoms occupy all the octahedral and tetrahedral voids formed by the *fcc*-type Sb sublattice. Hence, the Sb/Zn/Li/Li atomic layers produced a stacking sequence of ABC along the [111]<sub>c</sub> direction after full Li intercalation (Supporting Information Figure S8). Figure 2c shows an atomic resolution HAADF image recorded at a lithiated region with the two phases intergrown inside one nanoparticle. The image above the red dotted line shows

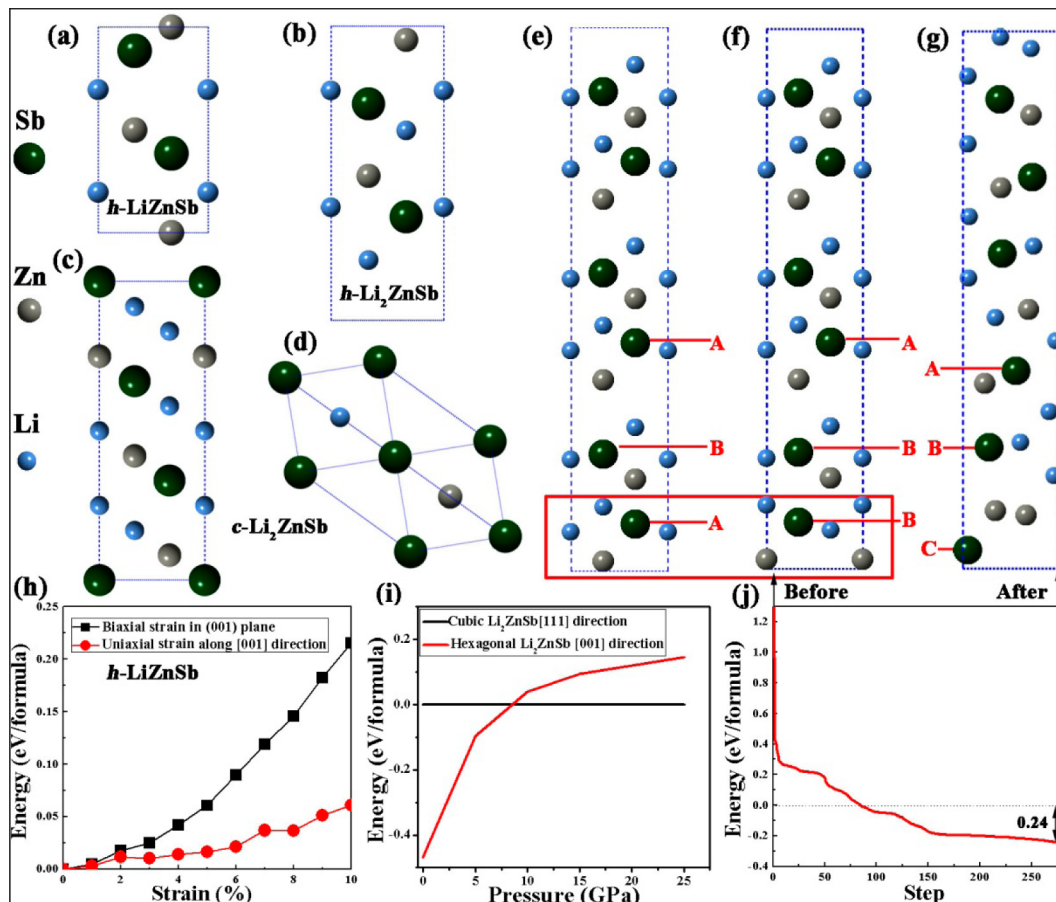


**Figure 4.** Ab initio simulations of phase transition from *h*-LiZnSb to *c*-Li<sub>2</sub>ZnSb. (a) Atomic structure of primitive cell of *h*-LiZnSb viewed along [100]<sub>h</sub>. (b) Atomic structure of primitive cell of *h*-Li<sub>2</sub>ZnSb viewed along [100]<sub>h</sub>. (c) Supercell of *c*-Li<sub>2</sub>ZnSb viewed along [110]<sub>c</sub>. (d) Atomic structure of primitive cell of *c*-Li<sub>2</sub>ZnSb viewed along [111]<sub>c</sub>. (e) 1 × 1 × 3 supercell of *h*-Li<sub>2</sub>ZnSb. (f) Supercell of *h*-Li<sub>2</sub>ZnSb by sliding one LiLiZnSb layer along [110]<sub>h</sub> direction before relaxation. The bottom Sb layer was moved from A site to B site. (g) Supercell of *h*-Li<sub>2</sub>ZnSb by sliding one LiLiZnSb layer after relaxation. The bottom Sb layer trends to occupy C site after relaxation. (h) Energy-strain curve of *h*-LiZnSb under biaxial strain in (001)<sub>h</sub> plane and uniaxial strain along [001]<sub>h</sub> direction. (i) Energy evolution by applying pressure along *h*-Li<sub>2</sub>ZnSb [001] direction and *c*-Li<sub>2</sub>ZnSb [111]<sub>c</sub> direction. (j) Energy evolution of relaxation of structure in (f).

hexagonally arranged bright atomic columns, which is characteristic for the AB stacked *h*-LiZnSb phase projected along the [001]<sub>h</sub> direction. The image below the red dotted line shows the existence of additional atomic columns at the center of hexagonal shaped atomic columns. Since Li ions are completely invisible by a HAADF detector due to their low scattering ability, the atomic columns observed at the centers of the hexagons corresponds to Sb or Zn atomic column occupied at the C sites and are indicative of the formation of the *c*-Li<sub>2</sub>ZnSb or Li<sub>3</sub>Sb domains projected along the [111]<sub>c</sub> direction. The cubic domain structure is further determined to be *c*-Li<sub>2</sub>ZnSb by the energy dispersive X-ray spectroscopy (EDS) analysis due to the presence of Zn atoms and HAADF images viewing along another zone axis (Supporting Information Figure S9). In Figure 2c, notably, Sb/Zn atomic columns at the C sites are less bright near the domain boundary compared with those equivalent sites in the *c*-Li<sub>2</sub>ZnSb domain below, which can be possibly explained by the presence of the inclined diffusional interface that is not parallel to the (010)<sub>h</sub> plane. Perfect coherent relationship between the two phases indicates nearly zero interfacial strain and is essential for a high interface mobility during lithium intercalation associated with the phase transition kinetics.<sup>26,27</sup> Figure 2d shows an atomic resolution HAADF image recorded after the interface swept across the

region. The whole domain is occupied by *c*-Li<sub>2</sub>ZnSb structure projected with [111]<sub>c</sub> direction with ABC stacking sequence.

Figure 3 provides a different view of the lithiation induced reordering of the stacked atoms between *h*-LiZnSb and *c*-Li<sub>2</sub>ZnSb from their respective [100]<sub>h</sub> and [110]<sub>c</sub> zone axes. From this projection, the crystallographic positions (i.e., ABC sites) of different atomic layers belonging to either hexagonal or cubic phases can be straightforwardly viewed based on their relative displacement along the [120]<sub>h</sub>/[112]<sub>c</sub> directions. Figure 3a shows an atomic HAADF image of the *h*-LiZnSb structure viewed along the [100]<sub>h</sub> direction. In Figure 3a, the brighter atomic columns can be clearly identified as Sb sites from the Z-contrast HAADF image and the Sb sublattice exhibits the A<sub>Sb</sub>B<sub>Sb</sub> stacking mode. Upon further lithiation, we observed new structural domains (marked as I, II, and III) that are sandwiched by neighboring A<sub>Sb</sub>B<sub>Sb</sub>-stacked atomic layers and deviate from the pristine *h*-LiZnSb structure (Figure 3b). These domains correspond to several A<sub>Sb</sub>B<sub>Sb</sub>C<sub>Sb</sub>-stacked atomic layers, which appear in the typical cubic *fcc* phase. Partial dislocation cores ( $b = 1/3 \langle 120 \rangle$ ), which were observed in the middle between Domain III and its left part, indicate transient displacement of the atomic layer between the AB and ABC stacking domains due to partial lithiation. The lithiation continues until all the A<sub>Sb</sub>B<sub>Sb</sub> stacks belonging to *h*-LiZnSb

phase are transformed to new  $A_{Sb}B_{Sb}C_{Sb}$  stacking mode in *c*-Li<sub>2</sub>ZnSb phase (Figure 3c). Figure 3d–f show the strain mappings along the stacking direction ([001]<sub>*h*</sub> or [111]<sub>*c*</sub>) derived by geometric phase analysis (GPA)<sup>28</sup> from the HAADF images of Figure 3a–c. In the pristine *h*-LiZnSb and fully lithiated *c*-Li<sub>2</sub>ZnSb (Figure 3d and f), there is no obvious strain fluctuation. At the initial lithiation stage of *h*-LiZnSb (Figure 3e), it is surprising to note that those AB-stacked domains undergo large tensile strain (as measured *d* spacing  $\sim$  3.84 Å) while the newly formed ABC-stacked ones experience great compressive strain (*d* spacing  $\sim$  3.52 Å, i.e., I, II, and III domains in Figure 3b), assuming that the upper left region is unlithiated and has a zero strain. Despite the fact that perfect *c*-Li<sub>2</sub>ZnSb phase should have a larger *hkl* interlayer spacing (3.74 Å) than that (3.57 Å) of the *h*-LiZnSb phase, we here attribute the increased interlayer separation of *h*-LiZnSb domains to the effect of partial Li intercalation at initial lithiation stage. The lithiation occurs at different layers and forms highly tensile domains due to the facilitated intercalation and diffusion of the lithium ions along the (001)<sub>*h*</sub> planes.<sup>29</sup> Those nonintercalated domains sandwiched between neighboring partially lithiated domains would thus experience great compressive stresses, which account for the rearrangements of the atomic layers and alternation of their stacking order as observed in the domains I, II, and III. Further lithiation in the rearranged domains with shuffled atomic stacks (i.e., domains I, II, and III) eventually drive all the atomic layers to the ABC stacked Li<sub>2</sub>ZnSb cubic phase, and is accompanied by the bulk stress relief through volume expansion. Based on these experimental observations, a hypothetical mechanism of the lithiation induced crystalline–crystalline phase transition is proposed here in Figure 3g. Owing to the highly anisotropic lithiation kinetics in *h*-LiZnSb that has more closely packed Sb atomic layers on the (001) plane, the in-plane lithium diffusion is expected to be much faster than the out-of-plane lithium hopping between different Sb layers. Such inhomogeneous intercalation of the lithium between the layered Sb sublattice leads to a sandwich geometry consisting of intercalated (Li<sub>2</sub>ZnSb) and nonintercalated (LiZnSb) lamellar domains. Here, the formulas of Li<sub>2</sub>ZnSb and LiZnSb only represent nonintercalated and intercalated domains, respectively. These intercalated domains maintain their stacking order well but experience a remarkable uniaxial expansion along the [001] direction, which induces a giant compressive stress on their neighboring nonintercalated domains and shuffles the atomic stacks in these domains. Subsequent lithium-ion intercalation into these rearranged domains in return gives a compressive stress on the lithiated *h*-Li<sub>2</sub>ZnSb ones and cause similar atomic displacement. Continuous lithiation results in the back and forth “breathing-like” lattice expansion and contraction in nanodomains that are coupled with the rearrangement of atomic stacks. Following such a “shuffling” mechanism, fully lithiated *c*-Li<sub>2</sub>ZnSb nanophases locating at an energy minimum would start to nucleate, and eventually lead to the formation of bulk *c*-Li<sub>2</sub>ZnSb crystals with a global volume expansion. This phase transition mechanism would lead to an orientation relationship of  $\langle 120 \rangle\{001\}h\text{-LiZnSb} // \langle 11\bar{2} \rangle\{111\}c\text{-Li}_2\text{ZnSb}$ , which is also supported by the experimentally observed orientation relationship between the *h*-LiZnSb and *c*-Li<sub>2</sub>ZnSb domains (Supporting Information Figure S10).

Ab initio simulations help to provide theoretical evidence for our proposed “shuffling” mechanism for the lithiation-induced *h*-LiZnSb to *c*-Li<sub>2</sub>ZnSb phase transition, as shown in Figure 4a

and 4e. Figure 4h shows the energy-strain curve of *h*-LiZnSb under biaxial strain in the (001)<sub>*h*</sub> plane and uniaxial strain along the [001]<sub>*h*</sub> direction. The energy required for uniaxial strain along the [001]<sub>*h*</sub> direction is much smaller than that for biaxial strain in the (001)<sub>*h*</sub> plane, which suggests Li ion is easier to intercalate and diffuse between the (001)<sub>*h*</sub> planes, which coincides well with our experimental observations. This is also similar to Li intercalation in layered materials, such as graphite.<sup>30</sup> In addition, the energy-strain curve also suggests that the lattice expands more along the [001]<sub>*h*</sub> direction than in the (001)<sub>*h*</sub> plane, which provides a simple explanation why coexistence of the *h*-LiZnSb and *c*-Li<sub>2</sub>ZnSb phases results in perfect coherency viewed along the [001]<sub>*h*</sub> direction (Figure 2c) and strain fluctuations viewed along the [100]<sub>*h*</sub> direction (Figure 3b, e).

Figure 4a–j provides a more in-depth understanding on why *h*-Li<sub>2</sub>ZnSb structure does not form as a stable phase during lithiation. Figure 4b shows a hypothetical situation where Li intercalation results in *h*-Li<sub>2</sub>ZnSb formation. This consideration is in conflict with our observation that Li<sub>2</sub>ZnSb is in the cubic phase. According to our HAADF imaging (Figure 2 and Figure 3), the correspondent lattice parameters of *h*-LiZnSb and *c*-Li<sub>2</sub>ZnSb are close. We constrain the lattice parameters of hexagonal and cubic Li<sub>2</sub>ZnSb as that of pristine *h*-LiZnSb with applying pressure along the [001]<sub>*h*</sub> and [111]<sub>*c*</sub> directions. The total energy of *h*-Li<sub>2</sub>ZnSb is 0.17 eV/formula larger than that of *c*-Li<sub>2</sub>ZnSb by calculation (Figure 4i). Therefore, the *h*-Li<sub>2</sub>ZnSb is a metastable phase during Li intercalation under constrain and should transform to cubic phase to lower the total energy. The transition from *h*-Li<sub>2</sub>ZnSb to *c*-Li<sub>2</sub>ZnSb can be explained by the sliding mechanism as shown in Figure 4e–f. The *h*-Li<sub>2</sub>ZnSb contains two layers of Li in the (001)<sub>*h*</sub> plane. Due to weak interaction between Li layers and the Zn/Sb layer, it is expected that the sliding of different layers in the (001)<sub>*h*</sub> plane is energy favorable. By sliding one LiLiZnSb layer along [110]<sub>*h*</sub> direction (the Sb layer sliding from A site to B site), as shown in Figure 4e and f, we find that the system energy reduced by 0.24 eV/formula and the Sb layers preferred to present ABC stacking sequence after relaxation shown in Figure 4e and g. Therefore, we claim that the *h*-Li<sub>2</sub>ZnSb is energetically unfavorable and it will transform to *c*-Li<sub>2</sub>ZnSb by layer sliding. In fact, the phase transition from hexagonal to cubic crystals has been reported in nanoclusters, such as CdSe.<sup>31,32</sup> The transition is attributed to sliding of parallel planes driven by pressure.

In summary, we reported here a new mechanism by which Li ions induced phase transitions in the host electrode. Using atomic resolution STEM and observing the real time dynamics of lithiation process in ZnSb single crystals, we observed that the *h*-LiZnSb transferred into *c*-Li<sub>2</sub>ZnSb structure instead of a direct transition to Li<sub>3</sub>Sb. The two phases of LiZnSb and Li<sub>2</sub>ZnSb have a coherent interfacial structure with a  $\langle 120 \rangle\{001\}h\text{-LiZnSb} // \langle 11\bar{2} \rangle\{111\}c\text{-Li}_2\text{ZnSb}$  corresponding relationship. According to the experimental evidence, we propose that basal atom layer is “shuffled” caused by the local lithium ion intercalation in the *h*-LiZnSb lattice. This results in the phase transition from *h*-LiZnSb to *c*-Li<sub>2</sub>ZnSb.

The observation of new mechanism for Li-induced crystalline–crystalline phase transition indicates that more comprehensive theories explaining the structural change in crystalline electrode materials need to be developed. This observed mechanism can also be applicable to other layered electrode materials developed for new battery chemistries including sodium or multivalent systems. The correlation of

atoms with the electrochemical behavior provides deeper insight into the atomic pathway of phase transitions opening new opportunities to develop high performance rechargeable batteries.

## ■ ASSOCIATED CONTENT

### Supporting Information

Experimental details and additional figures and movies. This material is available free of charge via the Internet at <http://pubs.acs.org>

## ■ AUTHOR INFORMATION

### Corresponding Author

\*E-mail: Reza@mtu.edu.

### Author Contributions

<sup>§</sup>These authors contribute equally.

### Notes

The authors declare no competing financial interest.

## ■ ACKNOWLEDGMENTS

R.S.-Y. acknowledges the financial support from the National Science Foundation (Awards No. CMMI-1200383 and DMR-1410560) and the American Chemical Society-Petroleum Research Fund (Award No. 51458-ND10). The acquisition of the UIC JEOL JEM-ARM200CF is supported by an MRI-R<sup>2</sup> grant from the National Science Foundation (Award No. DMR-0959470). Support from the UIC Research Resources Center is also acknowledged.

## ■ REFERENCES

- (1) Armand, M.; Tarascon, J.-M. *Nature* **2008**, *451*, 652–657.
- (2) Poizot, P.; Laruelle, S.; Gruegeon, S.; Dupont, L.; Tarascon, J. *Nature* **2000**, *407*, 496–499.
- (3) Chan, C. K.; Peng, H.; Liu, G.; McIlwrath, K.; Zhang, X. F.; Huggins, R. A.; Cui, Y. *Nat. Nanotechnol.* **2007**, *3*, 31–35.
- (4) Tarascon, J.-M.; Armand, M. *Nature* **2001**, *414*, 359–367.
- (5) Bruce, P. G.; Freunberger, S. A.; Hardwick, L. J.; Tarascon, J.-M. *Nat. Mater.* **2011**, *11*, 19–29.
- (6) Delmas, C.; Maccario, M.; Croguennec, L.; Le Cras, F.; Weill, F. *Nat. Mater.* **2008**, *7*, 665–671.
- (7) Yamada, A.; Koizumi, H.; Nishimura, S.-i.; Sonoyama, N.; Kanno, R.; Yonemura, M.; Nakamura, T.; Kobayashi, Y. *Nat. Mater.* **2006**, *5*, 357–360.
- (8) McDowell, M. T.; Lee, S. W.; Harris, J. T.; Korgel, B. A.; Wang, C.; Nix, W. D.; Cui, Y. *Nano Lett.* **2013**, *13*, 758–764.
- (9) Huang, J. Y.; Zhong, L.; Wang, C. M.; Sullivan, J. P.; Xu, W.; Zhang, L. Q.; Mao, S. X.; Hudak, N. S.; Liu, X. H.; Subramanian, A. *Science* **2010**, *330*, 1515–1520.
- (10) Liu, X. H.; Wang, J. W.; Huang, S.; Fan, F.; Huang, X.; Liu, Y.; Krylyuk, S.; Yoo, J.; Dayeh, S. A.; Davydov, A. V. *Nat. Nanotechnol.* **2012**, *7*, 749–756.
- (11) Gao, Q.; Meng, G.; Nie, A.; Mashayek, F.; Wang, C.; Odegard, G. M.; Shahbazian-Yassar, R. *Chem. Mater.* **2014**, 1660.
- (12) Gu, M.; Wang, Z.; Connell, J. G.; Perea, D. E.; Lauhon, L. J.; Gao, F.; Wang, C. *ACS Nano* **2013**, *7*, 6303–6309.
- (13) Zhu, Y.; Wang, J. W.; Liu, Y.; Liu, X.; Kushima, A.; Liu, Y.; Xu, Y.; Mao, S. X.; Li, J.; Wang, C. *Adv. Mater.* **2013**, *5461*–5466.
- (14) Park, C. M.; Sohn, H. J. *Adv. Mater.* **2010**, *22*, 47–52.
- (15) Zhao, X.; Cao, G. *Electrochim. Acta* **2001**, *46*, 891–896.
- (16) Xu, J.; Wu, H.; Wang, F.; Xia, Y.; Zheng, G. *Adv. Energy Mater.* **2013**, *3*, 286–289.
- (17) Fernández-Madrigal, F. J.; Lavela, P.; Vicente, C. P.; Tirado, J. L.; Jumas, J. C.; Olivier-Fourcade, J. *Chem. Mater.* **2002**, *14*, 2962–2968.
- (18) Aldon, L.; Garcia, A.; Olivier-Fourcade, J.; Jumas, J.-C.; Fernández-Madrigal, F. J.; Lavela, P.; Vicente, C. P.; Tirado, J. L. *J. Power Sources* **2003**, *119*, 585–590.
- (19) Morcrette, M.; Larcher, D.; Tarascon, J.-M.; Edström, K.; Vaughey, J.; Thackeray, M. *Electrochim. Acta* **2007**, *52*, 5339–5345.
- (20) Nie, A.; Gan, L.-Y.; Cheng, Y.; Asayesh-Ardakani, H.; Li, Q.; Dong, C.; Tao, R.; Mashayek, F.; Wang, H.-T.; Schwingenschlögl, U. *ACS Nano* **2013**, *7*, 6203–6211.
- (21) Klie, R. F.; Qiao, Q.; Paulauskas, T.; Ramasse, Q.; Oxley, M. P.; Idrobo, J. *Phys. Rev. B* **2012**, *85*, 054106.
- (22) Oshima, Y.; Sawada, H.; Hosokawa, F.; Okunishi, E.; Kaneyama, T.; Kondo, Y.; Niitaka, S.; Takagi, H.; Tanishiro, Y.; Takayanagi, K. *J. Electron Microsc.* **2010**, *59*, 457–461.
- (23) Gu, L.; Zhu, C.; Li, H.; Yu, Y.; Li, C.; Tsukimoto, S.; Maier, J.; Ikuhara, Y. *J. Am. Chem. Soc.* **2011**, *133*, 4661–4663.
- (24) Ishikawa, R.; Okunishi, E.; Sawada, H.; Kondo, Y.; Hosokawa, F.; Abe, E. *Nat. Mater.* **2011**, *10*, 278–281.
- (25) Hartel, P.; Rose, H.; Dinges, C. *Ultramicroscopy* **1996**, *63*, 93–114.
- (26) Puri, S.; Wadhawan, V. *Kinetics of phase transitions*; CRC Press: Boca Raton, FL, 2009.
- (27) Meethong, N.; Huang, H.; Speakman, S. A.; Carter, W. C.; Chiang, Y. M. *Adv. Funct. Mater.* **2007**, *17*, 1115–1123.
- (28) Hjøtt, M.; Snoeck, E.; Kilaas, R. *Ultramicroscopy* **1998**, *74*, 131–146.
- (29) Persson, K.; Hinuma, Y.; Meng, Y. S.; Van der Ven, A.; Ceder, G. *Phys. Rev. B* **2010**, *82*, 125416.
- (30) Shu, Z.; McMillan, R.; Murray, J. *J. Electrochem. Soc.* **1993**, *140*, 922–927.
- (31) Wang, Z.; Wen, X.-D.; Hoffmann, R.; Son, J. S.; Li, R.; Fang, C.-C.; Smilgies, D.-M.; Hyeon, T. *Proc. Natl. Acad. Sci. U. S. A.* **2010**, *107*, 17119–17124.
- (32) Wickham, J. N.; Herhold, A. B.; Alivisatos, A. *Phys. Rev. Lett.* **2000**, *84*, 923.